Combined Effects of Midlevel Dry Air and Vertical Wind Shear on Tropical Cyclone Development. Part II: Radial Ventilation

JOSHUA J. ALLAND,[a] BRIAN H. TANG,[b] KRISTEN L. CORBOSIERO,[b] AND GEORGE H. BRYAN[a]

[a] *National Center for Atmospheric Research, Boulder, Colorado*
[b] *Department of Atmospheric and Environmental Sciences, University at Albany, State University of New York, Albany, New York*

(Manuscript received 27 February 2020, in final form 2 December 2020)

ABSTRACT: This study demonstrates how midlevel dry air and vertical wind shear (VWS) can modulate tropical cyclone (TC) development via radial ventilation. A suite of experiments was conducted with different combinations of initial midlevel moisture and VWS environments. Two radial ventilation structures are documented. The first structure is positioned in a similar region as rainband activity and downdraft ventilation (documented in Part I) between heights of 0 and 3 km. Parcels associated with this first structure transport low–equivalent potential temperature air inward and downward left of shear and upshear to suppress convection. The second structure is associated with the vertical tilt of the vortex and storm-relative flow between heights of 5 and 9 km. Parcels associated with this second structure transport low–relative humidity air inward upshear and right of shear to suppress convection. Altogether, the modulating effects of radial ventilation on TC development are the inward transport of low–equivalent potential temperature air, as well as low-level radial outflow upshear, which aid in reducing the areal extent of strong upward motions, thereby reducing the vertical mass flux in the inner core, and stunting TC development.

KEYWORDS: Atmosphere; Tropical cyclones; Convective-scale processes; Numerical analysis/modeling

1. Introduction

a. Review of Part I

Alland et al. (2021, hereafter referred to as Part I) utilized idealized, three-dimensional model simulations to document the effects of downdraft ventilation on tropical cyclone (TC) development within a bivariate parameter space of moisture and vertical wind shear (VWS). A strong, positive, linear relationship existed between the area-averaged, low-level vertical mass flux in the inner 75 km (defined as the inner core) and TC intensity. This linear increase was due to an increased areal extent of strong upward motions (defined as $w > 0.5\,\mathrm{m\,s^{-1}}$), and motivated an investigation of how downdraft ventilation modulates the areal extent of strong upward motions and TC intensity.

The three-dimensional structure of downdraft ventilation was associated with the vertical tilt of the vortex. Downdraft ventilation was located within, and cyclonically downstream of, rainband convection and cyclonically downstream from the vertical tilt direction. In addition, downdraft ventilation was stronger for a larger vertical tilt, associated with a weaker TC embedded in a drier and a higher-VWS environment, and extended from the surface to a height of 3 km.

Trajectories from downdraft ventilation regions showed recovery of low–equivalent potential temperature (θ_e) air, demonstrating that parcels entering the inner core can have high θ_e and do not inhibit convection downshear. Instead, the inhibitive effects of downdraft ventilation on TC development were the downward transport of low-θ_e, negative-buoyancy air, and low-level outflow upshear, which reduce the areal extent of strong upward motions left of shear and in the upshear semicircle, decrease the vertical mass flux in the inner core, and stunt TC development.

b. Literature review of radial ventilation

Part I focused on downdraft ventilation, but radial ventilation has also been shown to affect TC development (e.g., Tang and Emanuel 2012). In previous literature, radial ventilation has generally been called "midlevel ventilation," but the terminology is changed here to encompass radial inflow that transports low-θ_e air at *any* vertical level, not solely at midlevels. Radial ventilation involves the dilution of the high-θ_e air in the inner core with low-θ_e air intruding from the environment via storm-relative flow (Simpson and Riehl 1958; Willoughby et al. 1984; Bender 1997). Riemer and Montgomery (2011) provide a conceptual framework for radial ventilation by investigating the flow topology of air around TCs. A set of streamlines, called manifolds, divide the flow around a TC into distinct regions. The dividing streamline separates the area of rotation-dominated flow from the larger-scale environment and captures the location of the moist-θ_e envelope around a TC. The shape of the moist envelope is governed to first order by storm-relative flow. For strong TCs, the moist envelope is better protected from storm-relative flow and the intrusion of environmental dry air via the deflection by the swirling winds. For weak TCs, storm-relative environmental flow can more easily intrude into the moist envelope via radial ventilation. Fu et al. (2019) found that radial ventilation aloft may be more important for upper-layer VWS environments, while the pathway

Supplemental information related to this paper is available at the Journals Online website: https://doi.org/10.1175/JAS-D-20-0055.s1.

Corresponding author: Joshua J. Alland, jalland@ucar.edu

DOI: 10.1175/JAS-D-20-0055.1

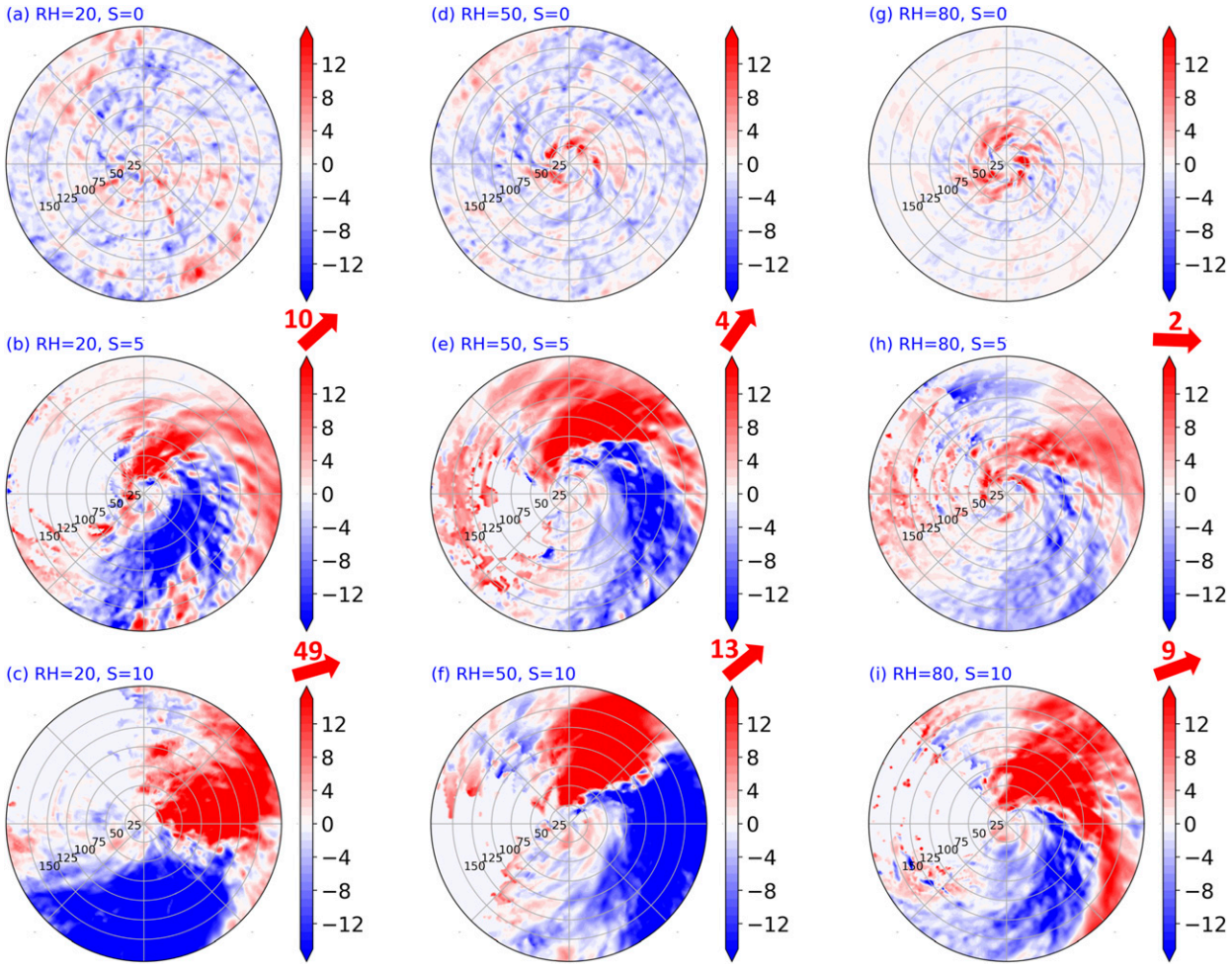

FIG. 1. Radial ventilation (kg K $m^{-2} s^{-1}$) at a height of 1 km across the bivariate parameter space. Red shading means radially inward motion of anomalously low-θ_e air. Each panel is time averaged during the bifurcation time period. The vertical tilt magnitude (km) and direction between the surface and a height of 6 km, time averaged during the bifurcation time period, are represented by the red number and arrow, respectively, for the experiments with VWS at the top right of each panel. Recall that the VWS direction is westerly for all experiments. Range rings are every 25 km.

documented in Part I may be more important for lower-layer shear. Observational case studies (Marks et al. 1992; Shelton and Molinari 2009) have related radial ventilation at midlevels to the weakening of TCs. A modeling case study by Cram et al. (2007) found that radial ventilation at midlevels reduced the eyewall θ_e by roughly 1 K for a mature TC. Here we seek to analyze the effects of radial ventilation on weak TCs for a variety of VWS and moisture environments, and at various vertical levels.

Didlake and Houze (2013) documented a potentially separate radial ventilation pathway in Hurricane Rita (2005), which had strong descending radial inflow associated with a stratiform rainband. The inflow was associated with low-θ_e air at both mid- and low levels, and may have transported this air into convection (e.g., radial ventilation) or downward into the subcloud layer (e.g., downdraft ventilation). Riemer et al. (2010) and Riemer and Montgomery (2011) showed that low-level, storm-relative flow consistently transports low-θ_e environmental air into this inflow region. A detailed study is necessary to document the importance of this radial ventilation pathway, and the connection between radial and downdraft ventilation in the descending radial inflow, on TC development for a variety of VWS and moisture environments.

c. *Purpose of this study*

This study investigates the effects of radial ventilation on TC development, and the structural dependence of radial ventilation on VWS and moisture. Questions addressed include the following: Is the three-dimensional structure of radial ventilation tied to the tilt of the vortex, as was found for downdraft ventilation in Part I? How does the three-dimensional structure of radial ventilation modulate the areal extent of strong upward motions, which Part I found to be directly correlated with TC development? An increased understanding of this potential relationship would help to better connect the influence of radial ventilation, which can affect the vertical mass flux, on TC intensity.

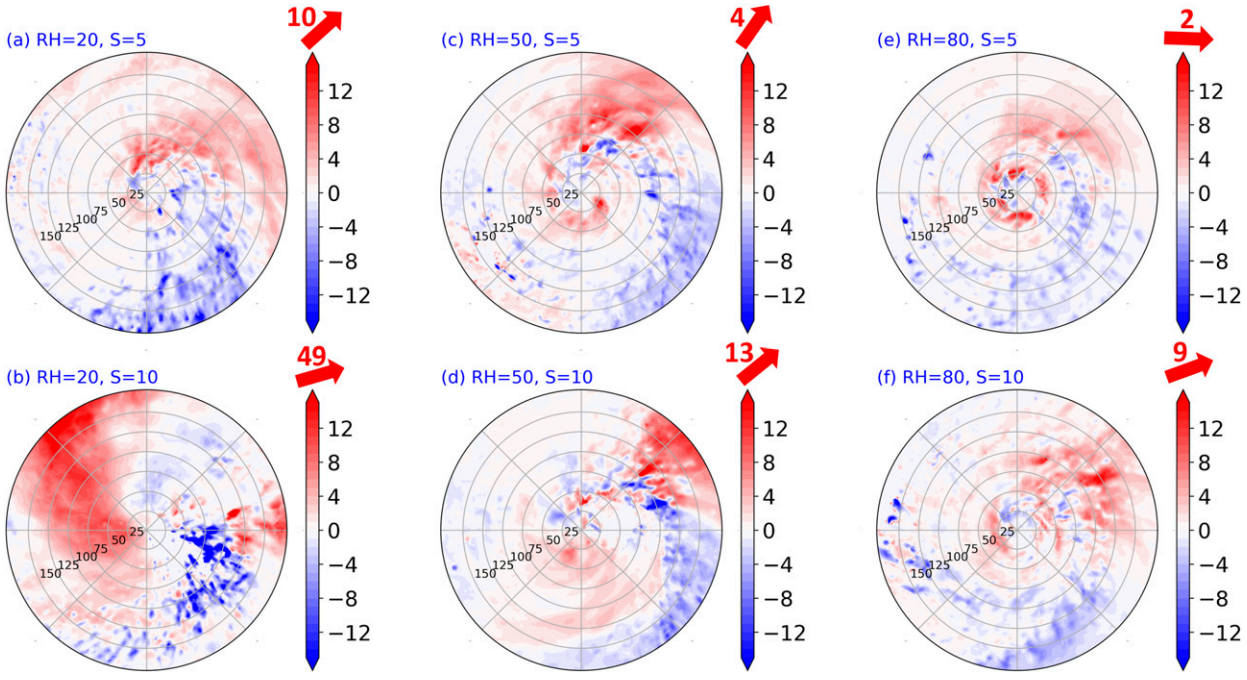

FIG. 2. As in Fig. 1, but at a height of 3 km. The S00 experiments are not shown. Recall that the VWS direction is westerly for all experiments.

Section 2 describes the moisture–VWS parameter space of experiments introduced in Part I. Part I demonstrated that processes affecting the vertical mass flux, such as radial ventilation, may affect TC development. This result motivates the investigation of radial ventilation by examining its three-dimensional structure in section 3 and its effects on convection in section 4. Section 5 analyzes the modulating effects of radial ventilation on upward motions in the inner core. Section 6 summarizes this study with conceptual diagrams.

2. Description of the experiments

Part I described the three-dimensional model, Cloud Model 1 (CM1), including the grid structure, initialization, and parameterization schemes utilized. The moisture–VWS bivariate parameter space consists of nine experiments with different combinations of initial relative humidity (RH)—20%, 50%, and 80% above 850 hPa—and westerly VWS—0, 5, and 10 m s^{-1} from 850 to 200 hPa. Below 850 hPa, the RH is set to the moist tropical temperature profile of Dunion (2011) for each experiment. The wind is zero below 850 hPa and is constant above 200 hPa. Part I describes how VWS is added. There is no VWS during the first 12 h to allow a realistic vortex to spin up with convection. After 12 h, VWS is added gradually and fully implemented by 24 h. As in Part I, the experiments are labeled as RH*XX*S*YY*, where *XX* and *YY* are the initial RH and VWS, respectively (e.g., RH20S05 refers to the experiment with 20% RH above 850 hPa and 5 m s^{-1} of deep-layer vertical wind shear). Experimental sets with the same initial RH profile are labeled as RH*XX*. Also as in Part I, the inner core is defined as the inner 75 km with respect to the low-level center, where radial ventilation above the low-level center may inhibit the growth and maintenance of upright deep convection.

How does radial ventilation, and its effects on θ_e, modulate the areal extent of strong upward motions and the vertical mass flux in the inner core, which is highly correlated with TC intensity? To answer this question, the next section explores the three-dimensional structure of radial ventilation, and the subsequent section assesses the impact of air from radial ventilation regions on convection in the inner core. Figures in the next section are time averaged during the bifurcation time period, defined in Part I as the 12-h period when the intensities in each RH experimental set bifurcate from one another. These time periods extend from 36 to 48 h for the RH20 and RH50 experimental sets, and 24 to 36 h for the RH80 experimental set (Fig. 2 from Part I).

3. Radial ventilation

a. *Radial ventilation structure between heights of 1 and 3 km*

Radial ventilation is defined as $\rho u'\theta_e'$, where ρ is density, and u is radial velocity. Primes denote perturbations from the azimuthal mean. This term represents the radial eddy flux of θ_e into the inner core, as defined in Tang and Emanuel (2010). Radial ventilation is calculated only in locations where $u < 0$ to focus on the *inward* transport of low-θ_e air. Note that radial ventilation is defined with respect to the low-level center. When a vortex is tilted in the vertical, air at a higher altitude has a radial component with respect to the low-level center, meaning that environmental air could intrude into the inner core above the low-level center. This tilt-induced flow over the low-level center has been shown to be associated with

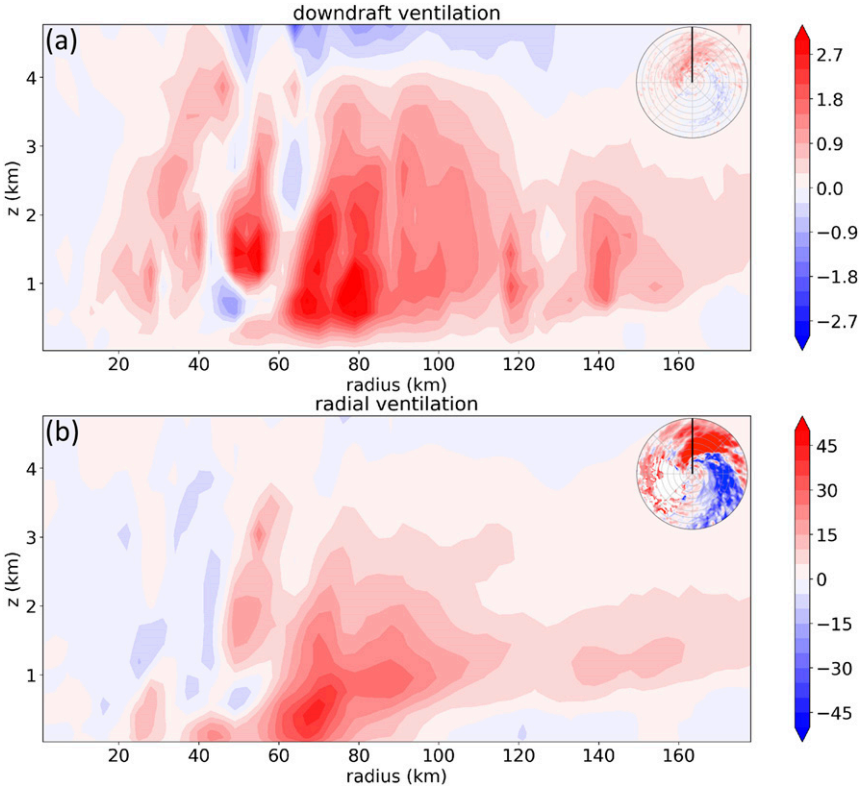

FIG. 3. North–south radial–vertical cross section of (a) downdraft and (b) radial ventilation (kg K $m^{-2} s^{-1}$) for RH50S05 time averaged during the bifurcation time period. The inset images show the respective ventilation structures at a height of 1 km for RH50S05 and the black line in each represents the location of the cross section. The range of values on the color bars differs compared to the inset for clarity.

nondevelopment (Rappin et al. 2010; Raymond et al. 2011; Davis and Ahijevych 2012). Sections 3a and 3b discuss the structure of radial ventilation between heights of 1–3 and 5–9 km, respectively, as these vertical layers have different radial ventilation structures.

Figure 1 shows the radial ventilation structure at an altitude of 1 km, time averaged during the bifurcation time period for each experiment. Note that both negative u' and θ_e' contribute to the radial ventilation structure. Our focus is on the positive (red) regions of radial ventilation because these regions are indicative of the transport of low-θ_e air inward to potentially frustrate TC development. No clear radial ventilation structure exists outside a radius of 75 km for the S00 experiments (Figs. 1a,d,g), so these experiments are omitted for now. For RH20S05 (Fig. 1b), radial ventilation is oriented azimuthally left of shear within the inner 100 km, and oriented downshear and downshear right (DR) outside of 100 km, while RH20S10 (Fig. 1c) has radial ventilation downshear. The RH50 (Figs. 1e,f) and RH80 (Figs. 1h,i) experimental sets have a radial ventilation structure oriented left of shear within the inner 100 km. This structure is similar to the downdraft ventilation structure in Part I and suggests downdraft and radial ventilation may be connected to the same physical phenomenon, namely, rainband activity, as suggested in Didlake and Houze (2013). The radial inflow pattern is potentially governed by radial buoyancy gradients discussed in Didlake and Houze (2013).

Figure 2 shows the radial ventilation structure at a height of 3 km. For most of the S05 and S10 experiments, the radial ventilation structures are similar to Fig. 1, but with lower magnitudes. This result is consistent with downdraft ventilation maximized below 3 km and further suggests that these two ventilation pathways in the lower troposphere are connected. To further explore this connection, Fig. 3 shows a north–south, radial–vertical cross section of downdraft (Fig. 3a) and radial (Fig. 3b) ventilation through the principal rainband for RH50S05 time averaged during the bifurcation time period. Both ventilation pathways are located below a height of 3 km, with positive values in roughly the same location, and maxima at a radius of 70 km. The combined structure of radial and downdraft ventilation results in a slantwise descent of low-θ_e air from a radius of 160 to 40 km. The other experiments show a similar ventilation structure (not shown).

For RH20S10, the radial ventilation structure is notably different at 3 km (Fig. 2b) compared to at 1 km (Fig. 1c). At 3 km, radial ventilation exists in the upshear-left (UL) quadrant and wraps radially inward to the upshear-right (UR) quadrant. Reasons for this distinct ventilation structure, which

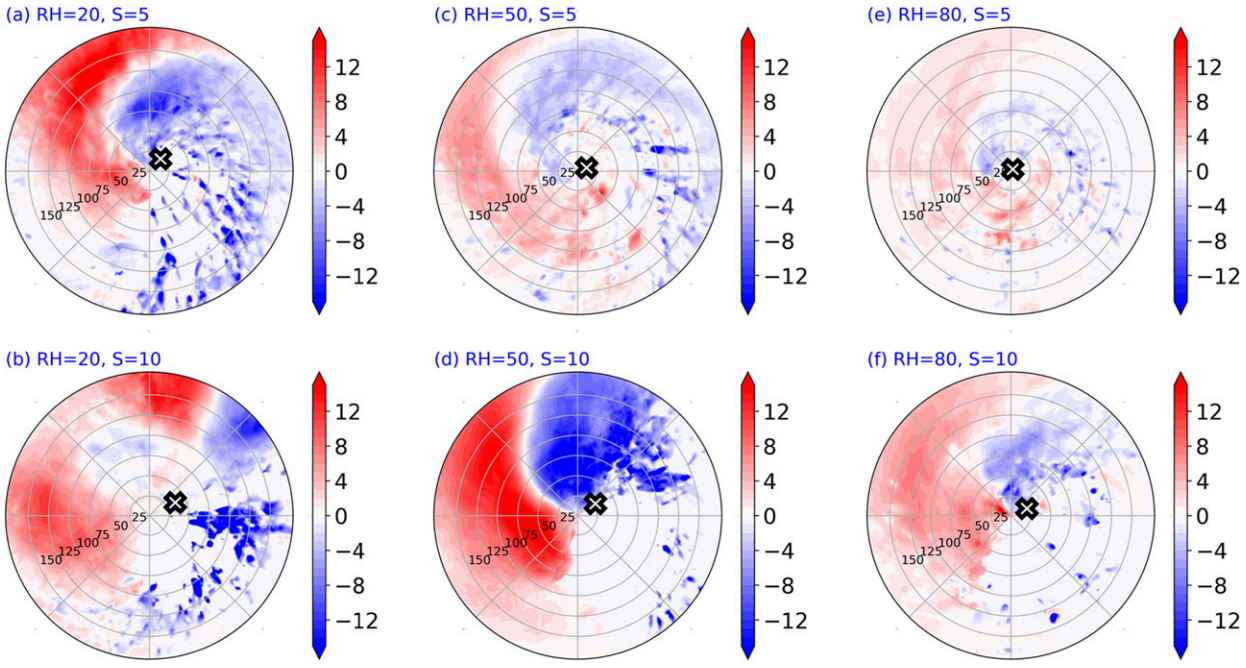

FIG. 4. As in Fig. 1, but at a height of 5 km. The white × in each panel represents the TC center at a height of 5 km.

appears in other experiments higher in the troposphere (5–9 km), will be analyzed in the next section.

b. *Radial ventilation structure between heights of 5 and 9 km*

Figure 4 shows the radial ventilation structure at a height of 5 km, time averaged during the bifurcation time period, for each experiment. A similar structure as RH20S10 in Fig. 2b exists for the S05 and S10 experiments. For the RH20 experimental set (Figs. 4a,b), RH20S05 has radial ventilation in the UL quadrant, wrapping radially inward to the UR quadrant. During the bifurcation time period, the vertical tilt in this experiment is directed downshear left (DL) (white ×). At a height of 5 km, a vertical tilt in this direction results in northwesterly flow over the low-level center as air rotates around the midlevel center. This radial ventilation pathway provides a different avenue, compared to that below 3 km, by which low-θ_e air can intrude into the inner core above the low-level center. RH20S10 shows a similar region of radial ventilation, although the positive values do not appear to wrap around from the UL to UR quadrants as coherently compared to RH20S05. Instead, radial ventilation is maximized in two locations, left of shear and upshear, potentially associated with the vertical tilt of the vortex and storm-relative flow, respectively.

The RH50 (Figs. 4c,d) and RH80 (Figs. 4e,f) experimental sets show similar structures of radial ventilation wrapping radially inward to the UR quadrant. These two sets have stronger radial ventilation for S10, associated with a larger vertical tilt and stronger storm-relative flow (not shown). For all experiments, this ventilation structure extends up to 9 km but is weaker than at 5 km (shown in the next subsection).

Overall, two different radial ventilation pathways are documented. The first pathway, lower in the troposphere, is associated with rainband activity. The second pathway, higher in the troposphere, is associated with the vertical tilt of the vortex and storm-relative flow.

c. *Radial ventilation at every vertical level*

Radial ventilation in Figs. 1–4 has a clear wavenumber-1 structure. To investigate the vertical structure of radial ventilation, an azimuthal Fourier decomposition of radial ventilation is performed at every height. Figure 5 shows azimuth–height diagrams of the wavenumber-1 component of radial ventilation radially averaged over the inner 150 km during the bifurcation time period. For each experiment, two clear radial ventilation structures exist that increase in strength as the VWS increases. At low levels, radial ventilation occurs between the surface and 3 km, and is associated with the location of the principal rainband and easterly storm-relative flow. Radial ventilation generally has a minimum in midlevels between heights of 3 and 4 km. This vertical layer represents a transition zone from rainband-induced radial ventilation to vertical tilt-induced radial ventilation, and is associated with near zero storm-relative flow (dashed black line in each panel). Above 4 km, radial ventilation increases and is maximized in the upshear semicircle for each experiment, and is associated with westerly storm-relative flow. The exception is RH20S10 (Fig. 5b), which transitions to the vertical tilt-induced radial ventilation pathway at a lower level of roughly 3 km, consistent with Fig. 2. In addition, the RH80 experimental set (Figs. 5e,f) has radial ventilation maximized at a slightly higher level of about 7 km. This pattern is attributed to a more vertically stacked vortex and a smaller vertical tilt magnitude at mid- to upper levels for higher relative humidity environments (not shown).

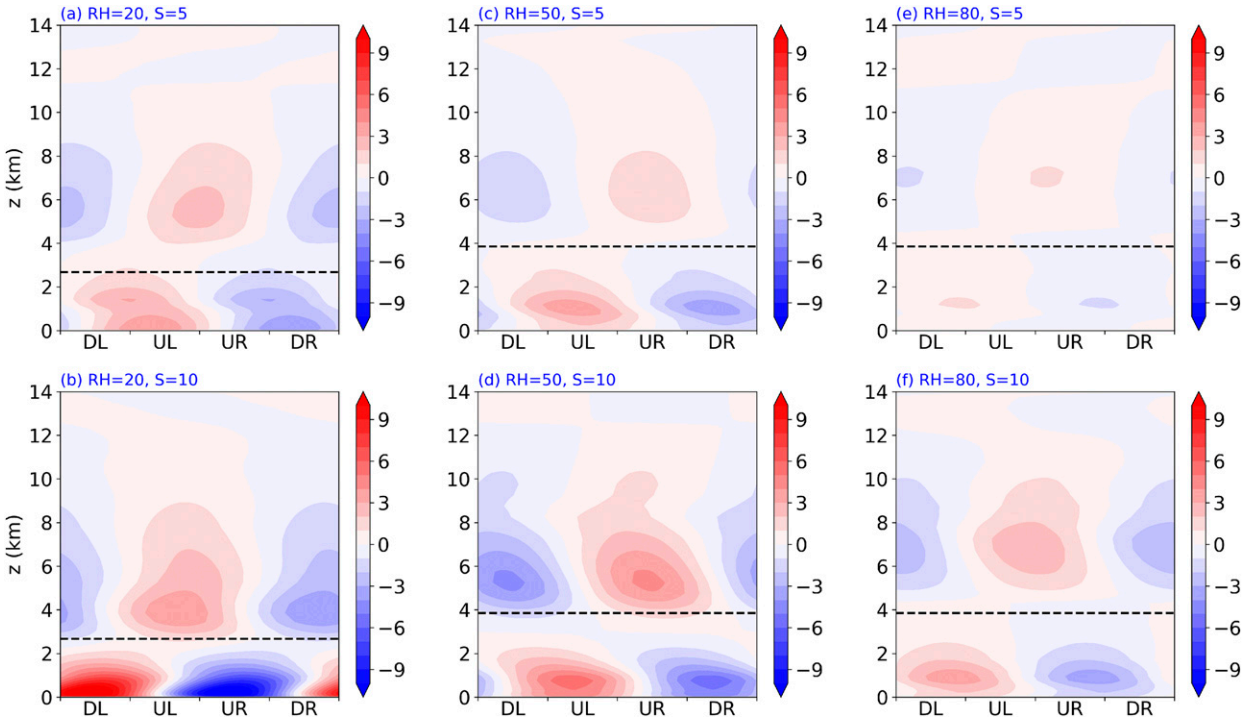

FIG. 5. Azimuth–height diagrams of the wavenumber-1 component of radial ventilation (kg K m^{-2} s^{-1}) within the bivariate parameter space. Radial ventilation is radially averaged within the inner 150 km and time averaged during the bifurcation time period. The dashed black line in each panel represents the height where the storm-relative flow changes from easterly below the black line to westerly above the black line.

In summary, these results shed light on the vertical structure of radial ventilation pathways. Radial ventilation between the surface and 3 km is associated with rainband activity and easterly storm-relative flow, and radial ventilation between 5 and 9 km is associated with the vertical tilt of the vortex and westerly storm-relative flow. The vertical structure of radial ventilation suggests that weaker TCs embedded in drier and higher VWS environments (and having larger vertical tilts) have stronger radial ventilation at all levels; however, does this low-θ_e air get transported radially inward and affect convection in the inner core? Does air from radial ventilation regions reduce the areal extent of strong upward motions, decrease the vertical mass flux in the inner core, and reduce TC intensity? Riemer and Montgomery (2011) suggested that much of the environmental air aloft may be deflected by the swirling winds and not intrude into the inner core, although for weak TCs, this environmental interaction may be stronger. The Eulerian analysis does not show if environmental air intrudes into the inner core. The next section utilizes trajectories to determine how air from radial ventilation regions affects the thermodynamics of individual parcels and convection in the inner core, similar to the objective in Cram et al. (2007).

4. Effects of radial ventilation on convection: Trajectory analyses

Similar to Part I, we used the Lagrangian Analysis Tool (Lagranto) to compute forward trajectories (Wernli and Davies 1997; Sprenger and Wernli 2015). Two sets of trajectories are utilized in this section and integrated forward in time for 24 h. First, trajectories were initialized in radial ventilation regions at heights of 1, 2, and 3 km, associated with rainband activity and easterly storm-relative flow, to determine how this air affects the distribution of convection. Second, trajectories were initialized in radial ventilation regions at heights of 5, 6, 7, 8, and 9 km, associated with the vertical tilt of the vortex and westerly storm-relative flow, to determine how this air affects the distribution of convection. The online supplement contains animations of the parcels comprising the trajectories for each set.

a. *Trajectories in radial ventilation regions between heights of 0 and 3 km*

Figure 6 presents the initialization locations of trajectories in radial ventilation regions for the S05 and S10 experiments at heights of 1, 2, and 3 km, and within the inner 180 km on the left-of-shear side, which capture the structure of radial ventilation in Figs. 1 and 2. Trajectories are analyzed only for an initial radial ventilation magnitude of at least 5 kg K m^{-2} s^{-1} to focus on the strongest radial ventilation regions in the principal rainband region. Table 1 lists the number of trajectories for each experiment. The variability in the number of trajectories across experiments reflects differences in the areal coverage of radial ventilation (Figs. 1 and 2).

Figure 7 shows the normalized trajectory density for parcels below a height of 3 km during the 24-h integration. For the RH20 experimental set (Figs. 7a,b), RH20S05 has a stream of trajectories that rotates cyclonically about the TC center.

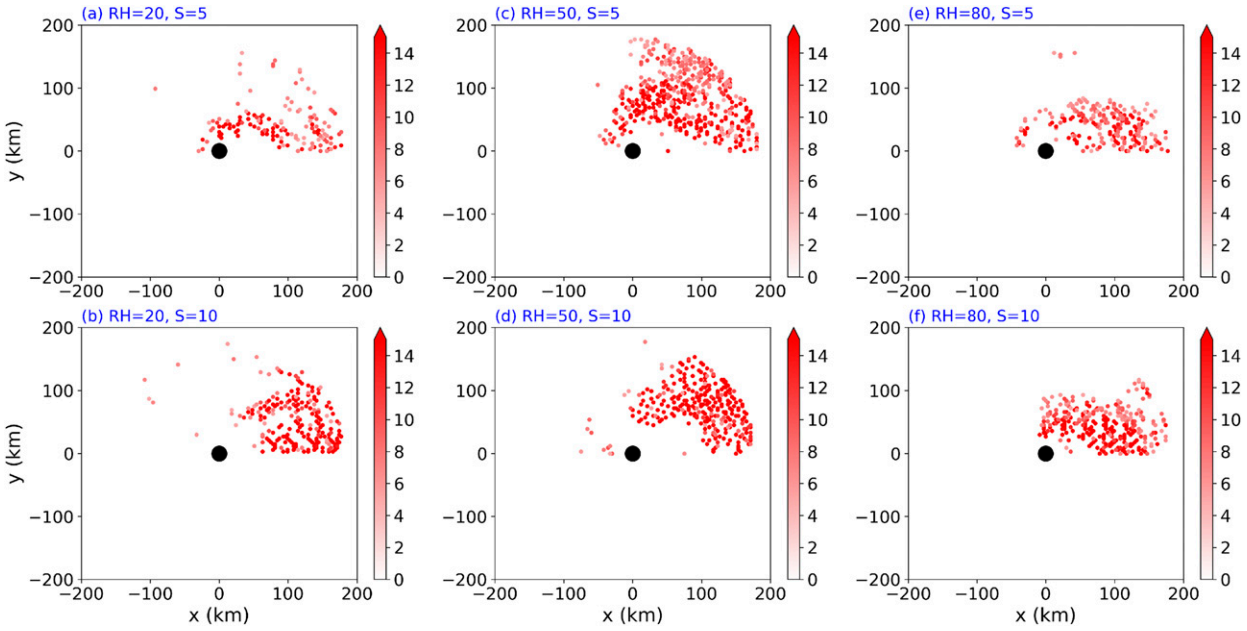

FIG. 6. Trajectory initialization locations (red dots) in radial ventilation (kg K m^{-2} s^{-1}). Trajectories were initialized at the beginning of each bifurcation time period, at heights of 1, 2, and 3 km, within the inner 180 km on the left-of-shear side, and for an initial radial ventilation magnitude of at least 5 kg K m^{-2} s^{-1}. Additional trajectories were initialized hourly during the first 6 h. Every 10 trajectory initialization locations at heights of 1, 2, and 3 km are plotted. The black dot in each panel represents the center of the TC at the lowest model level.

Upon reaching the UL quadrant, these parcels are transported outward due to radial outflow associated with the dynamic response of a tilted vortex (Fig. 13 in Part I). Once reaching right of shear, parcels are transported radially inward in an inflow corridor. RH20S10 has trajectories that are initialized more downshear and radially outward compared to trajectories in RH20S05 (Fig. 6). Similar to RH20S05, however, most parcels move to the UL quadrant and are transported radially outward. Two streams of trajectories exist (s_1 and s_2), and these streams extend outward to larger radii compared to RH20S05. This result is due to stronger radial outflow in RH20S10 (Fig. 13 in Part I), associated with the dynamic response of a vortex having a larger vertical tilt. Note that the evolution in the RH20 experimental set closely matches the evolution of the downdraft ventilation trajectories from Fig. 12 in Part I.

For the RH50 experimental set (Figs. 7c,d), RH50S05 has a stream of trajectories that is transported cyclonically within the inner 50 km, while another stream of trajectories is transported cyclonically outside of the inner core. The parcels extending to larger radii (>50 km) are transported radially outward upshear and form an inflow corridor in the DR quadrant. RH50S10 has multiple trajectory streams. The streams extend farther from the TC center compared to RH50S05, and are associated with greater radial outflow in the UR quadrant (Fig. 13 in Part I). The parcels form a similar inflow corridor in the DR quadrant.

For the RH80 experimental set (Figs. 7e,f), the majority of parcels in RH80S05 stay within the inner 100 km while rotating cyclonically about the TC center. A secondary stream of trajectories is located radially outward from the primary stream, but this secondary stream does not extend radially outward like in the RH20 and RH50 experimental sets, due to the much smaller vertical tilt. RH80S10 shows a similar pattern as RH80S05, albeit with a broader areal extent of low trajectory density upshear.

To determine if trajectories from radial ventilation regions reach the inner core with low θ_e to potentially inhibit convection, Fig. 8 presents the average θ_e of trajectories below 3 km during the 24-h integration. Overall, the pattern for each experiment looks similar to the downdraft ventilation trajectories from Fig. 16 in Part I, although the average θ_e is less in the inflow corridor downshear for each experiment compared to in Part I. This result is likely because parcels extend up to 3 km, as opposed to only 1 km from Fig. 16 in Part I, encompassing parcels above the boundary layer away from the direct effect of surface fluxes. The similarity between the downdraft and radial ventilation trajectories provide further evidence that these two ventilation pathways are connected and closely tied to rainband activity (Didlake and Houze 2013).

b. *Trajectories in radial ventilation regions between heights of 5 and 9 km*

To investigate radial ventilation at middle and upper levels, trajectories were initialized at the beginning of the bifurcation time period, at heights of 5, 6, 7, 8, and 9 km, within the inner 180 km on the upshear side, and for an initial radial ventilation magnitude of at least 2 kg K m^{-2} s^{-1} (Fig. 9). Additional trajectories were initialized hourly during the first 6 h. Table 2 presents the number of trajectories for each experiment. Many more trajectories were initialized compared to the previous sets of trajectories due to the larger areal coverage of radial

TABLE 1. Number of trajectories initialized in radial ventilation regions in the inner 180 km at heights of 1, 2, and 3 km. Initialization occurs at the beginning of the bifurcation time period for each experiment and trajectories were integrated forward for 24 h with output every minute. Additional trajectories were initialized hourly during the first 6 h.

Experiment	Number of trajectories
RH20S05	1428
RH20S10	2143
RH50S05	4868
RH50S10	2886
RH80S05	2176
RH80S10	2981

ventilation at each height, and at a greater number of vertical levels. RH80S05 has fewer trajectories initialized due to the weaker, narrower region of radial ventilation compared to the other experiments (Fig. 4e).

Figure 10 shows the normalized trajectory density for parcels that stay above a height of 2 km during the integration period. For each panel, parcels within the pink circle are within the inner core with respect to the low-level center. Table 2 lists the average residence time for parcels in the upshear and right-of-shear inner core. The residence time describes how long air from radial ventilation regions stays within the inner core, where a longer residence time means that dry air stays within the inner core longer to potentially disrupt or inhibit convection. For the RH20 experimental set (Figs. 10a,b), RH20S05 has parcels beginning upshear that are transported close to the TC center (inward of 20 km). Parcels stay within the upshear and right-of-shear inner core for roughly 2.7 h. Most parcels rotate around the TC center to the DR and DL quadrants, and are transported eastward by storm-relative flow at upper levels in these quadrants. These parcels rotate around the mid- to upper-level TC center at heights of 5 to 9 km, which is positioned in the DL quadrant (white ×). Due to this vertical tilt and storm-relative flow, radial ventilation occurs close to the low-level center upshear and potentially inhibits the growth and maintenance of upright deep convection (e.g., Wong and Chan 2004; James and Markowski 2010; Tang and Emanuel 2010; Helms and Hart 2015). For RH20S10, parcels generally move eastward with time. The lack of rotation of these parcels compared to RH20S05 is due to weaker mid- and upper-level vortices for RH20S10 (not shown). As a result, radial ventilation occurs directly over the low-level center due to storm-relative flow, and parcels stay in the upshear and right-of-shear inner core for roughly 3 h, slightly longer than for RH20S05.

For the RH50 experimental set (Figs. 10c,d), RH50S05 has parcels that rotate cyclonically around the low-level center. The vertical tilt has a lower magnitude compared to RH20S05, and parcels remain farther away from the low-level center for RH50S05. Parcels have an average residence time of roughly 1.7 h, a reduction of about 1 h compared to RH20S05. RH50S10 has parcels that move closer to and over the low-level center with a longer average residence time compared to RH50S05, due to a larger vertical tilt and stronger storm-relative flow. The mid- and upper-level vortices are weaker compared to RH50S05 (not shown), so trajectories do not form a closed loop.

For the RH80 experimental set (Figs. 10e,f), RH80S05 has parcels that rotate around the low-level center, due to the relatively small vertical tilt compared to RH20S05 and RH50S05. For RH80S10, parcels follow a similar pattern as RH50S10, although parcels stay farther from the TC center and

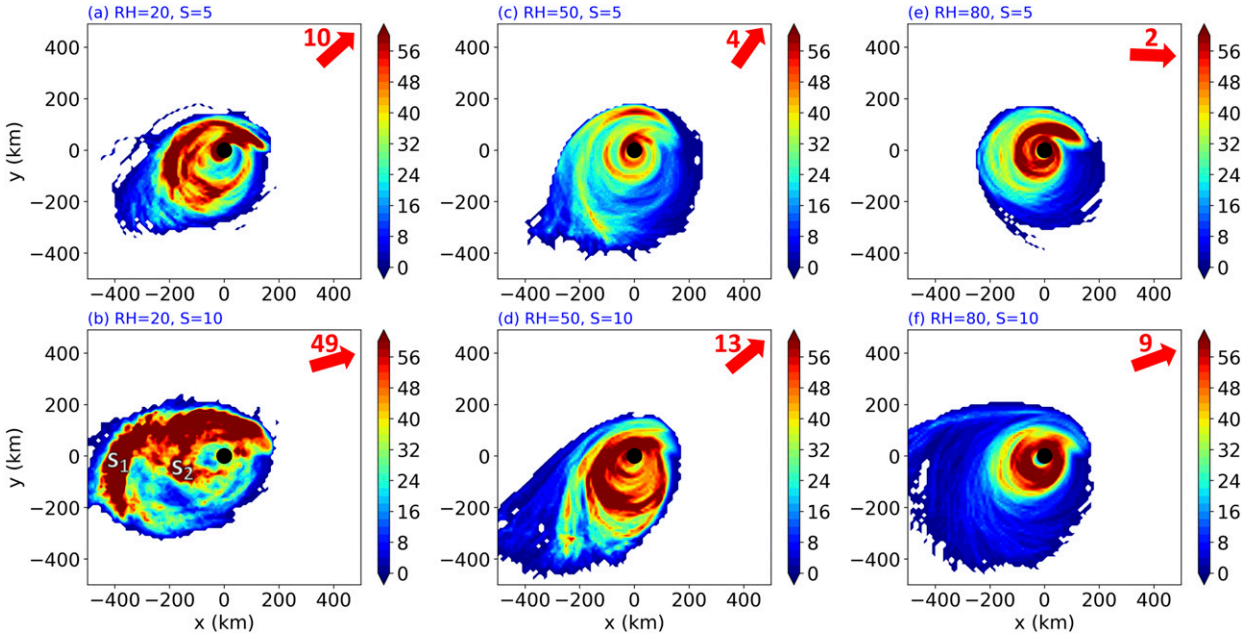

FIG. 7. Number of radial ventilation trajectories ($\times 10^{-2}$) from Fig. 6 passing through a location below a height of 3 km during the 24-h integration. The number has been normalized by the total number of trajectories initialized listed in Table 1.

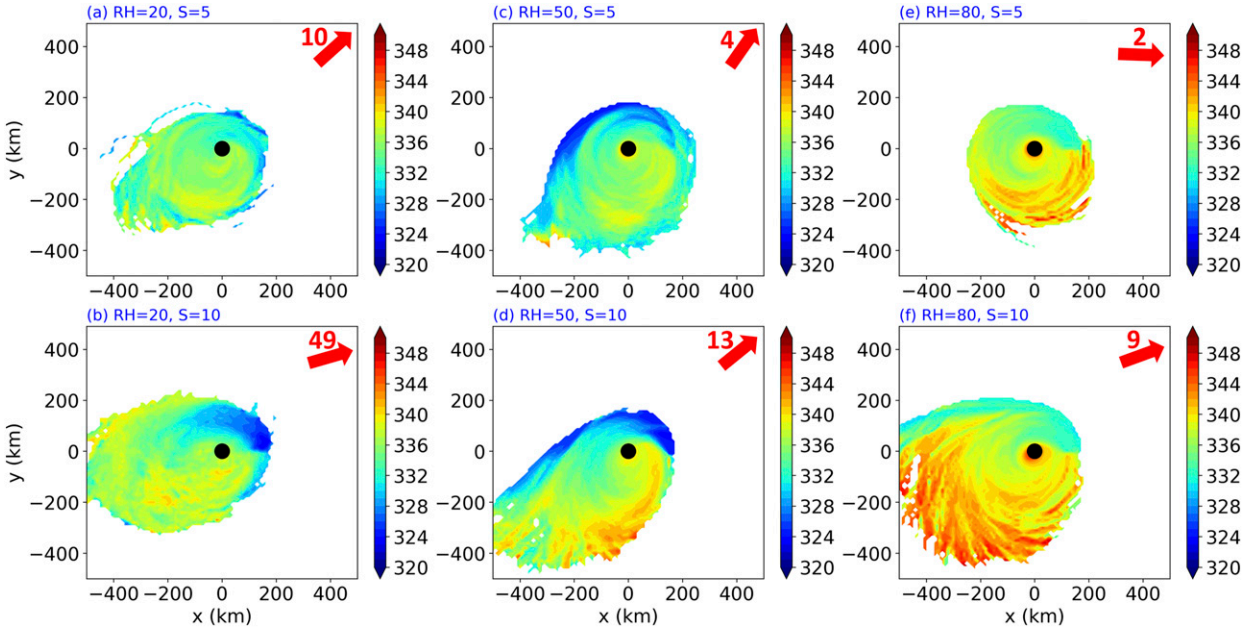

FIG. 8. As in Fig. 7, but for the average equivalent potential temperature (K).

have a shorter average residence time (1.5 h), due to the smaller vertical tilt.

Overall, the residence time is longer as the VWS magnitude increases (an exception is the RH80 experimental set). To better understand how radial ventilation modulates the distribution of dry air in the region above the low-level center, Fig. 11 presents the average RH of trajectories from Fig. 10. RH is presented here, instead of θ_e, because RH differences are larger aloft. In addition, the experimental setup has the initial RH constant with height in the environment. The environmental θ_e is not constant with height. Thus, RH is chosen because trajectories are averaged over heights that span from 5 to 9 km. Table 2 lists thermodynamic information of parcels in the upshear and right-of-shear inner core: the average RH of

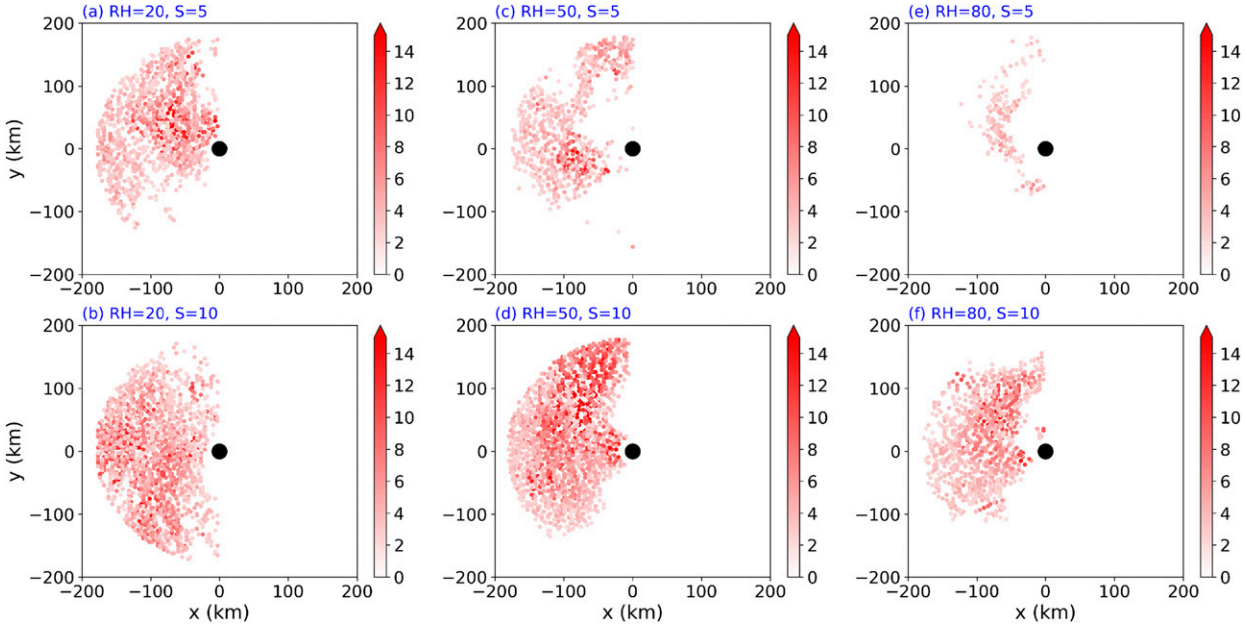

FIG. 9. Trajectory initialization locations (red dots) in radial ventilation (kg K m^{-2} s^{-1}). Trajectories were initialized at the beginning of each bifurcation time period, at heights of 5, 6, 7, 8, and 9 km, within the inner 180 km on the upshear side, and for an initial radial ventilation magnitude of at least 2 kg K m^{-2} s^{-1}. Every 10 trajectory initialization locations at heights of 5, 6, 7, 8, and 9 km are plotted. Every 10 trajectory initialization locations are plotted.

TABLE 2. Number of trajectories initialized in radial ventilation regions in the inner 180 km at heights of 5, 6, 7, 8, and 9 km. Initialization occurs at the beginning of the bifurcation time period for each experiment and trajectories were integrated forward for 24 h with output every minute. Additional trajectories were initialized hourly during the first 6 h. Residence time represents the average time parcels stay within the upshear and right-of-shear inner core. The average RH of these parcels is listed. The reduction in RH and θ_e represents the average difference between each trajectory in the inner core (at a given radius and height) and the time-averaged (during the bifurcation time period), azimuthally averaged value of the corresponding S00 experiment at the same height and radius.

Experiment	Number of trajectories	Residence time	Average RH	Reduction in RH (θ_e)
RH20S05	11 449	2.7 h	47.0%	−34.9% (−3.5 K)
RH20S10	16 800	3.0 h	33.3%	−47.8% (−6.4 K)
RH50S05	7199	1.7 h	68.4%	−23.1% (−3.4 K)
RH50S10	16 826	2.5 h	47.2%	−39.1% (−7.0 K)
RH80S05	1755	1.7 h	87.4%	−5.9% (−1.9 K)
RH80S10	10 114	1.5 h	72.6%	−17.3% (−3.3 K)

parcels and average difference in RH (and θ_e) between parcels at a given radius and height, and the time-averaged (during the bifurcation time period), azimuthally averaged value of the corresponding S00 experiment at the same radius and height. These quantities provide a thermodynamic estimate of the radial ventilation affects aloft in the inner core. For the RH20 experimental set (Figs. 11a,b), RH values between 30% and 50% exist in the upshear and right-of-shear inner core. RH20S05 has an average RH of 47% and a reduction in RH of 34.9% (θ_e of 3.5 K) compared to RH20S00. This low-RH air is transported to the DR quadrant, where the RH increases, likely due to mixing with moist parcels rising from below (Fig. 4 from Part I). RH20S10 shows a similar pattern, although the RH values are lower with an average RH of 33.3% and a reduction in RH of 47.8% (θ_e of 6.4 K). Many of these trajectories are transported directly over the TC center with a slightly longer residence time in the inner core, making the middle to upper levels inhospitable to deep convection immediately around the low-level TC center.

The RH50 (Figs. 11c,d) and RH80 (Figs. 11e,f) experimental sets also show relatively low-RH air in the upshear and right-of-shear inner core, albeit with higher RH values due to a more humid environment (see Table 2 for quantitative information). The RH50S05 and RH50S10 experiments have a reduction in RH of 23.1% and 39.1% (θ_e of 3.4 and 7 K), respectively, compared to RH50S00. The RH80S05 and RH80S10 experiments have a reduction in RH of 5.9% and 17.3% (θ_e of 1.9 and 3.3 K), respectively, compared to RH80S00. The RH upshear is further decreased below the environmental value by shear-induced subsidence (Zawislak et al. 2016), which is not shown. Overall, as the vertical tilt increases in the higher VWS experiments, lower-RH air is transported into the inner core aloft

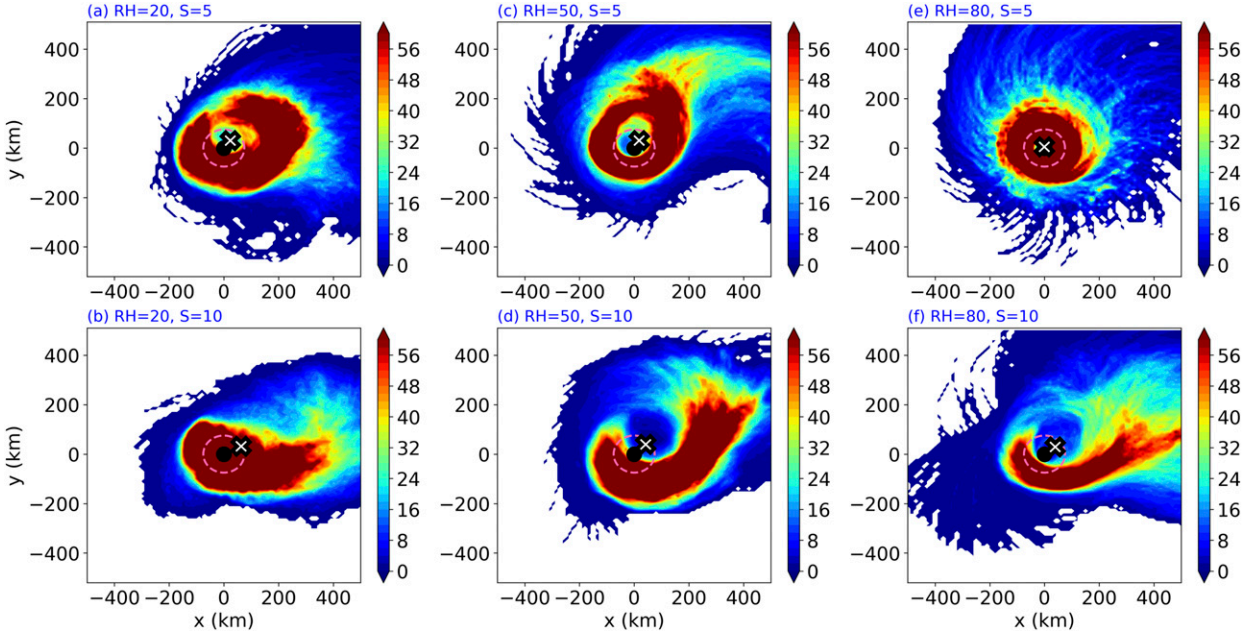

FIG. 10. Number of radial ventilation trajectories ($\times 10^{-2}$) from Fig. 9 passing through a location above 2 km during the 24-h integration. The number has been normalized by the total number of trajectories initialized listed in Table 2. The white × in each panel represents the TC center averaged between heights of 5 and 9 km. The dashed pink circle represents the inner core with respect to the low-level center.

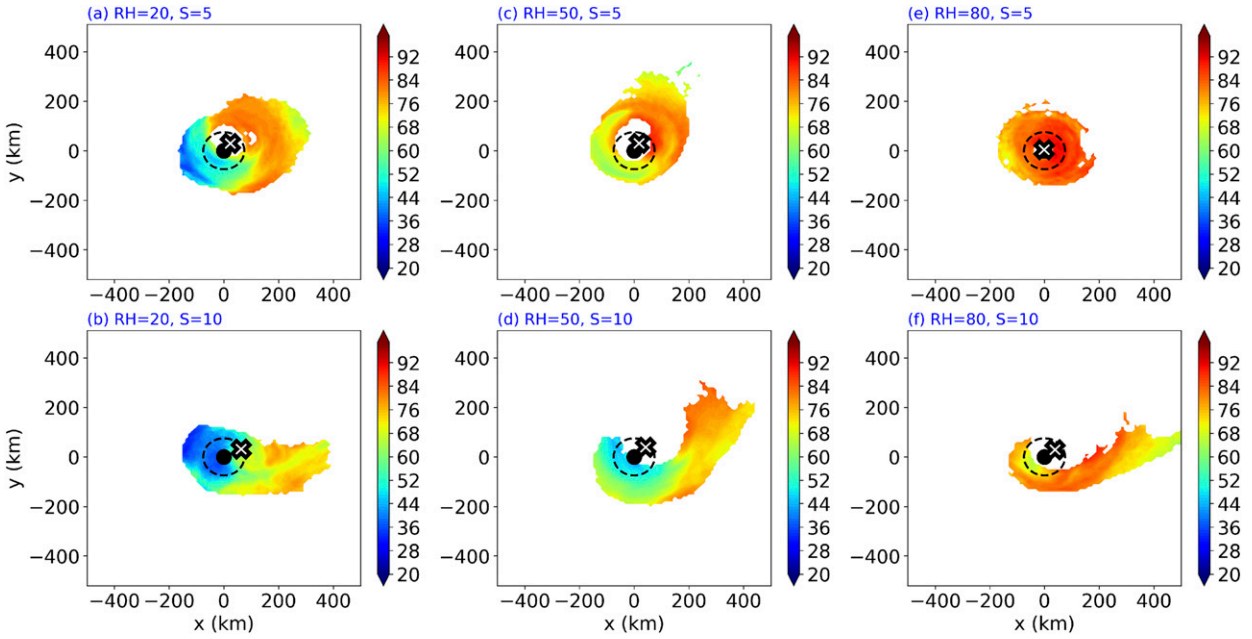

FIG. 11. As in Fig. 10, but for the average RH (%). Only the RH values that are associated with more than 4000 parcels passing through a point (from Fig. 10) are plotted. The dashed black circle represents the inner core with respect to the low-level center.

upshear and right of shear for a longer period of time. Such a radial ventilation pathway likely acts to inhibit convection in these locations, which is explored in the following section.

In summary, radial ventilation at low levels transports low-θ_e air inward consistently left of shear and in the upshear semicircle. In addition, radial ventilation at middle and upper levels transports low-RH air inward consistently upshear and to the right of shear. The next section addresses whether these ventilation pathways transport low-θ_e air into convection in the inner core to reduce the strength of upward motions.

5. Effects of radial ventilation on upward motions in the inner core

The time evolution of strong upward motions ($w > 0.5\,\mathrm{m\,s^{-1}}$) in the innermost 75 km of the UR quadrant is analyzed for each experiment to demonstrate the modulating effects of radial ventilation on convection and the development of a deep secondary circulation. Strong upward motions are analyzed because the areal extent of strong upward motions is strongly correlated with TC intensity in these experiments, discussed in Part I, and the UR quadrant is analyzed because this quadrant consistently experiences radial ventilation at middle to upper levels (Figs. 4 and 5). Figure 12 shows time–height diagrams of the spatially summed vertical mass flux of strong upward motions (shading), including only columns that have $w > 0.5\,\mathrm{m\,s^{-1}}$ at a height of 1 km, for the first 50 h of each experiment. For the S05 and S10 experiments, radial ventilation is shown in black contours for a value of $2\,\mathrm{kg\,K\,m^{-2}\,s^{-1}}$, and the numbers at the top right of each panel lists the percent decrease in vertical mass flux during the bifurcation time period in low levels (green boxes in Fig. 12) compared to the respective S00 experiment. The S00 experiments are shown for reference. For the RH20 experimental set (Figs. 12a–c), RH20S05 has positive vertical mass flux values periodically reaching above 3 km between 15 and 36 h. After 36 h, positive vertical mass flux values are predominately confined below 3 km, associated with radial ventilation between heights of 5 and 10 km, and the low-level vertical mass flux is reduced by 56% compared to RH20S00. RH20S10 shows a similar pattern of shallow upward motions with radial ventilation aloft after 36 h, and the low-level vertical mass flux is reduced by 74% compared to RH20S00.

The RH50 (Figs. 12d–f) and RH80 (Figs. 12g–i) experimental sets show a consistent evolution of the vertical mass flux values becoming shallower and radial ventilation aloft. In addition, the strength of the vertical mass flux at a height of 1 km decreases with time, particularly in the S10 experiments. The low-level vertical mass flux in the RH50S05 and RH50S10 experiments decreases by 50% and 92%, respectively, compared to RH50S00, while the low-level vertical mass flux in the RH80S05 and RH80S10 experiments decreases by 23% and 71%, respectively, suggesting that strong upward motions become less frequent in this quadrant as the VWS and radial ventilation aloft increases. In addition, downward motions develop between heights of 3 and 8 km for each experiment. Radial ventilation aloft likely contributes to the development of these downward motions, as well as shear-induced subsidence, and a continual stunting of convection in the UR quadrant occurs. Radial ventilation at middle to upper levels, thus, works in tandem with radial, and downdraft, ventilation at low levels to inhibit convection in the inner core by reducing the θ_e in the UR quadrant (Fig. 8, and Fig. 16 from Part I). The inhibition of strong upward motions and the lack of a deep

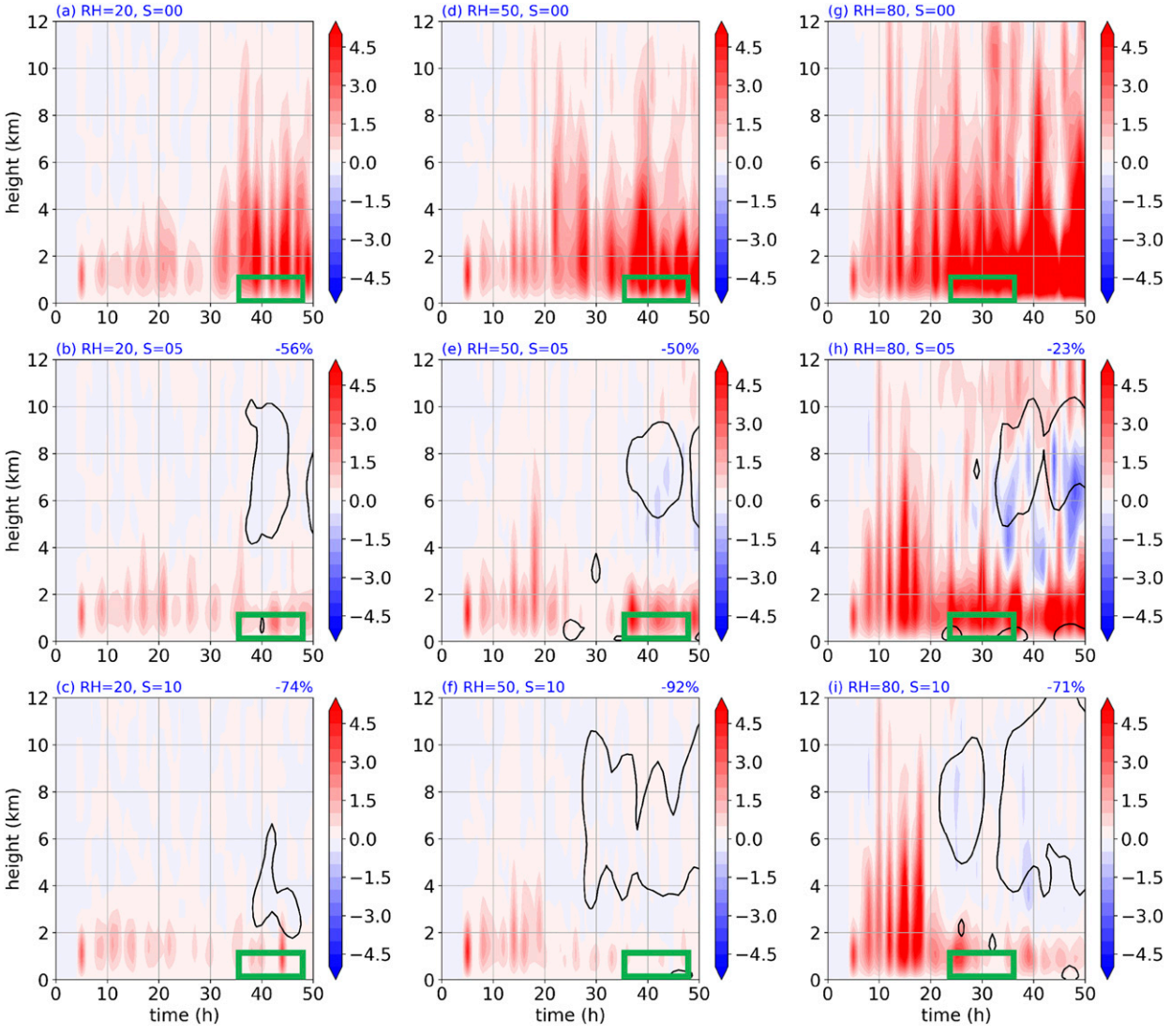

FIG. 12. Time–height diagrams of the vertical mass flux (shaded, $\times 10^{-3}$ kg m^{-2} s^{-1}) spatially summed for every column where strong upward motions exist, at a height of 1 km, in the UR inner core (radii < 75 km). For the S05 and S10 experiments, radial ventilation is shown in the black contours for a value of 2 kg K m^{-2} s^{-1}, smoothed using a two-dimensional Gaussian filter, and the top right of each panel lists the percentage decrease in vertical mass flux during the bifurcation time period in low levels (summed in the green box) compared to the respective S00 experiment. The S00 experiments are shown for reference.

secondary circulation limits the areal extent of strong upward motions in the inner core and stunts TC development.

6. Conclusions

This study discussed the effects of radial ventilation on reducing the vertical mass flux in the TC inner core and stunting TC development. The three-dimensional structure of radial ventilation did not show a clear structure for experiments without VWS (S00). For the experiments with VWS (S05 and S10), two radial ventilation pathways were documented. The first pathway was located at low levels (below 3 km) in the principal rainband region and was similar to the downdraft ventilation pathway documented in Part I. The second pathway was located above 5 km in the upshear semicircle and right of shear. This ventilation pathway was associated with the vertical tilt of the vortex and storm-relative flow, consistent with previous literature (Rappin et al. 2010; Raymond et al. 2011; Riemer and Montgomery 2011; Davis and Ahijevych 2012). The vertical structure of radial ventilation suggests that weaker TCs embedded in drier and higher VWS environments (and having larger vertical tilts) have stronger radial ventilation. These results expand on previous literature by documenting two different radial ventilation pathways, and how the structure and strength of these ventilation pathways change with different moisture and VWS environments.

To determine how radial ventilation modulated convection, two sets of forward trajectories were completed. The first set

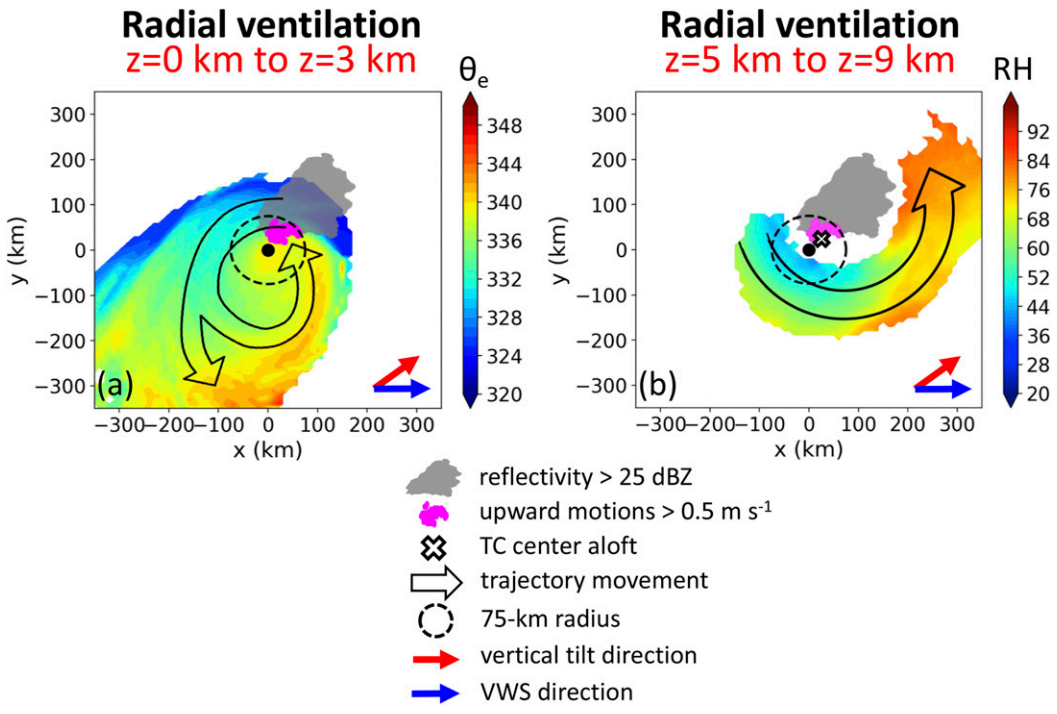

FIG. 13. Conceptual model of radial ventilation for RH50S10, adapted from Figs. 8 and 11 showing, in shading, the (a) average equivalent potential temperature (K) of trajectories initialized in radial ventilation regions between heights of 0 and 3 km, and (b) average RH (%) of trajectories initialized in radial ventilation regions between heights of 5 and 9 km. Other information includes reflectivity greater than 25 dBZ (gray shading), upward motions greater than 0.5 m s^{-1} (magenta dots), the TC center averaged between heights of 5 and 9 km (white ×), parcel movement (black arrows), the inner 75 km (dashed circle), the vertical tilt direction from the surface to 6 km (red arrow), and the VWS direction (blue arrow). The reflectivity and vertical velocity are time averaged during the bifurcation time period.

was initialized at heights of 1, 2, and 3 km to determine how radial ventilation, associated with rainband activity, affected the distribution of convection. Radial ventilation in the first set transported lower-θ_e air inward consistently left of shear as the VWS magnitude increased, and, along with low-level radial outflow upshear, suppressed convection left of shear and upshear. As documented in Didlake and Houze (2013), this pathway is collocated with downdraft ventilation in the principal rainband region. The second set was initialized at heights of 5, 6, 7, 8, and 9 km to determine how radial ventilation, associated with the vertical tilt of the vortex and storm-relative flow, affected the distribution of convection. Radial ventilation in the second set transported lower-RH air inward upshear and right of shear as the VWS magnitude increased to suppress convection.

The vertical mass flux in the UR inner core was analyzed to demonstrate the modulating effects of radial ventilation on convection. The vertical extent of positive vertical mass fluxes became shallower with a reduction in strong vertical velocities at low levels. The two radial ventilation pathways worked in tandem with low-level radial, and downdraft, ventilation to inhibit convection and a deep secondary circulation, limiting the areal extent of strong upward motions in the inner core, and stunting TC development.

A conceptual model of how radial ventilation modulates TC development is shown in Fig. 13 for RH50S10. Between heights of 0 and 3 km (Fig. 13a), trajectories initialized in radial ventilation regions, coinciding with convection (gray shading), are associated with low-θ_e air (colored shading). These parcels are transported cyclonically and radially outward in the upshear semicircle. The streams of trajectories and the evolution of θ_e look similar to the conceptual model of downdraft ventilation (Fig. 17 in Part I) due to the connection of downdraft and radial ventilation in the principal rainband region. Parcels that reach the inner core in the DR quadrant and downshear are associated with an increase in θ_e, and rise in strong upward motions (magenta dots).

Between heights of 5 and 9 km (Fig. 13b), trajectories initialized in radial ventilation regions are positioned in the upshear semicircle. These parcels are transported cyclonically about the middle- and upper-level vortices, and, due to the vertical tilt of the vortex and westerly storm-relative flow, transport low-RH air consistently into the upshear semicircle and right of shear in the inner core to suppress convection. These results show that for weak TCs, radial ventilation aloft is able to transport environmental air into the inner core, in agreement with the assertions set forth by Riemer and Montgomery (2011). Thus, the modulating effects of radial ventilation on TC development are the inward transport of low-θ_e and low-RH air from radial ventilation regions, along with low-level outflow upshear, which aid in reducing the areal extent of strong upward motions, thereby reducing the vertical mass flux in the inner core, and stunting TC development. Drier and higher-VWS

environments are generally associated with stronger radial and downdraft ventilation.

Future work should investigate if ventilation pathways operate differently during different stages and intensities of a TC's life cycle. The sensitivity of ventilation to other factors should be investigated, such as various sea surface temperatures, initial vortex sizes, wind profiles, VWS depths, and depths of dry air, to determine how these factors affect the structure of ventilation, and how ventilation modulates TC development. In addition, the three-dimensional structure of ventilation pathways documented in Part I and this study should be evaluated using observations and real-case model experiments. Last, future work should investigate if collecting and assimilating observations of moisture, temperature, and wind in ventilation regions, through the depth of the troposphere, provides forecast value.

Acknowledgments. This research was funded by National Science Foundation (NSF) Grant 1748779 and based upon work supported by the National Center for Atmospheric Research (NCAR), which is a major facility sponsored by the NSF under Cooperative Agreement 1852977. Joshua Alland was supported by NCAR's Advanced Study Program's Graduate Visitor Program and is currently supported by NCAR through an Advanced Study Program Postdoctoral Fellowship. Thank you to Michael Sprenger for creating a new version of Lagranto compatible with CM1. Thank you to Richard Rotunno for serving as an internal reviewer at NCAR. We would like to acknowledge high-performance computing support from Cheyenne provided by NCAR (Computational and Information Systems Laboratory 2017). Thank you to three anonymous reviewers for their suggestions to improve the contents of this manuscript.

REFERENCES

Alland, J. J., B. H. Tang, K. L. Corbosiero, and G. H. Bryan, 2021: Combined effects of midlevel dry air and vertical wind shear on tropical cyclone development. Part I: Downdraft ventilation. *J. Atmos. Sci.*, **78**, 763–782, https://doi.org/10.1175/JAS-D-20-0054.1.

Bender, M. A., 1997: The effect of relative flow on the asymmetric structure in the interior of hurricanes. *J. Atmos. Sci.*, **54**, 703–724, https://doi.org/10.1175/1520-0469(1997)054<0703:TEORFO>2.0.CO;2.

Computational and Information Systems Laboratory, 2017: Cheyenne: HPE/SGI ICE XA System (Climate Simulation Laboratory). National Center for Atmospheric Research, https://doi.org/10.5065/D6RX99HX.

Cram, T. A., J. Persing, M. T. Montgomery, and S. A. Braun, 2007: A Lagrangian trajectory view on transport and mixing processes between the eye, eyewall, and environment using a high-resolution simulation of Hurricane Bonnie (1998). *J. Atmos. Sci.*, **64**, 1835–1856, https://doi.org/10.1175/JAS3921.1.

Davis, C. A., and D. A. Ahijevych, 2012: Mesoscale structural evolution of three tropical weather systems observed during PREDICT. *J. Atmos. Sci.*, **69**, 1284–1305, https://doi.org/10.1175/JAS-D-11-0225.1.

Didlake, A. C., and R. A. Houze, 2013: Dynamics of the stratiform sector of a tropical cyclone rainband. *J. Atmos. Sci.*, **70**, 1891–1911, https://doi.org/10.1175/JAS-D-12-0245.1.

Dunion, J. P., 2011: Rewriting the climatology of the tropical North Atlantic and Caribbean Sea atmosphere. *J. Climate*, **24**, 893–908, https://doi.org/10.1175/2010JCLI3496.1.

Fu, H., Y. Wang, M. Riemer, and Q. Li, 2019: Effect of unidirectional vertical wind shear on tropical cyclone intensity change—Lower-layer shear versus upper-layer shear. *J. Geophys. Res. Atmos.*, **124**, 6265–6282, https://doi.org/10.1029/2019JD030586.

Helms, C. N., and R. E. Hart, 2015: The evolution of dropsonde-derived kinematic and thermodynamic structures in developing and nondeveloping Atlantic tropical convective systems. *Mon. Wea. Rev.*, **143**, 3109–3135, https://doi.org/10.1175/MWR-D-14-00242.1.

James, R. P., and P. M. Markowski, 2010: A numerical investigation of the effects of dry air aloft on deep convection. *Mon. Wea. Rev.*, **138**, 140–161, https://doi.org/10.1175/2009MWR3018.1.

Marks, F. D., Jr., R. A. Houze Jr., and J. F. Gamache, 1992: Dual-aircraft investigation of the inner core of Hurricane Norbert. Part I: Kinematic structure. *J. Atmos. Sci.*, **49**, 919–942, https://doi.org/10.1175/1520-0469(1992)049<0919:DAIOTI>2.0.CO;2.

Rappin, E. D., D. S. Nolan, and K. A. Emanuel, 2010: Thermodynamic control of tropical cyclogenesis in environments of radiative-convective equilibrium with shear. *Quart. J. Roy. Meteor. Soc.*, **136**, 1954–1971, https://doi.org/10.1002/qj.706.

Raymond, D. J., S. L. Sessions, and C. López Carrillo, 2011: Thermodynamics of tropical cyclogenesis in the northwest Pacific. *J. Geophys. Res.*, **116**, D18101, https://doi.org/10.1029/2011JD015624.

Riemer, M., and M. T. Montgomery, 2011: Simple kinematic models for the environmental interaction of tropical cyclones in vertical wind shear. *Atmos. Chem. Phys.*, **11**, 9395–9414, https://doi.org/10.5194/acp-11-9395-2011.

——, ——, and M. E. Nicholls, 2010: A new paradigm for intensity modification of tropical cyclones: Thermodynamic impact of vertical wind shear on the inflow layer. *Atmos. Chem. Phys.*, **10**, 3163–3188, https://doi.org/10.5194/acp-10-3163-2010.

Shelton, K. L., and J. Molinari, 2009: Life of a six-hour hurricane. *Mon. Wea. Rev.*, **137**, 51–67, https://doi.org/10.1175/2008MWR2472.1.

Simpson, R., and R. Riehl, 1958: Mid-tropospheric ventilation as a constraint on hurricane development and maintenance. *Tech. Conf. on Hurricanes*, Amer. Meteor. Soc., Miami Beach, FL, D4-1–D4-10.

Sprenger, M., and H. Wernli, 2015: The Lagranto Lagrangian analysis tool—Version 2.0. *Geosci. Model Dev.*, **8**, 2569–2586, https://doi.org/10.5194/gmd-8-2569-2015.

Tang, B., and K. Emanuel, 2010: Midlevel ventilation's constraint on tropical cyclone intensity. *J. Atmos. Sci.*, **67**, 1817–1830, https://doi.org/10.1175/2010JAS3318.1.

——, and ——, 2012: Sensitivity of tropical cyclone intensity to ventilation in an axisymmetric model. *J. Atmos. Sci.*, **69**, 2394–2413, https://doi.org/10.1175/JAS-D-11-0232.1.

Wernli, B. H., and H. C. Davies, 1997: A Lagrangian-based analysis of extratropical cyclones. I: The method and some applications. *Quart. J. Roy. Meteor. Soc.*, **123**, 467–489, https://doi.org/10.1002/qj.49712353811.

Willoughby, H. E., F. D. Marks, and R. J. Feinberg, 1984: Stationary and moving convective bands in hurricanes. *J. Atmos. Sci.*, **41**, 3189–3211, https://doi.org/10.1175/1520-0469(1984)041<3189:SAMCBI>2.0.CO;2.

Wong, M. L. M., and J. C. L. Chan, 2004: Tropical cyclone intensity in vertical wind shear. *J. Atmos. Sci.*, **61**, 1859–1876, https://doi.org/10.1175/1520-0469(2004)061<1859:TCIIVW>2.0.CO;2.

Zawislak, J., H. Jiang, G. R. Alvey, E. J. Zipser, R. F. Rogers, J. A. Zhang, and S. N. Stevenson, 2016: Observations of the structure and evolution of Hurricane Edouard (2014) during intensity change. Part I: Relationship between the thermodynamic structure and precipitation. *Mon. Wea. Rev.*, **144**, 3333–3354, https://doi.org/10.1175/MWR-D-16-0018.1.